ARL-TR-10024 ● Nov 2024

Elucidating Single-Cell and Network Dynamics in Primary Hippocampal Cultures: Calcium Imaging and Analytic Methods

by Alexandra S Carrizales, Ian M Berke, Lowella V Fortuno, Patrick D Skelton, and Ann Mae DiLeonardi

NOTICES

Disclaimers

The findings in this report are not to be construed as an official Department of the Army position unless so designated by other authorized documents.

Citation of manufacturer's or trade names does not constitute an official endorsement or approval of the use thereof.

Destroy this report when it is no longer needed. Do not return it to the originator.

ARL-TR-10024 ● Nov 2024

Elucidating Single-Cell and Network Dynamics in Primary Hippocampal Cultures: Calcium Imaging and Analytic Methods

Alexandra S Carrizales, Lowella V Fortuno, and Patrick D Skelton
SURVICE Engineering Company

Ian M Berke and Ann Mae DiLeonardi
DEVCOM Army Research Laboratory

REPORT DOCUMENTATION PAGE

1. REPORT DATE	2. REPORT TYPE	3. DATES COVERED	
		START DATE	END DATE
November 2024	Technical Report	June 2022	August 2024

4. TITLE AND SUBTITLE
Elucidating Single-Cell and Network Dynamics in Primary Hippocampal Cultures: Calcium Imaging and Analytic Methods

5a. CONTRACT NUMBER	5b. GRANT NUMBER	5c. PROGRAM ELEMENT NUMBER
5d. PROJECT NUMBER	5e. TASK NUMBER	5f. WORK UNIT NUMBER

6. AUTHOR(S)
Alexandra S Carrizales, Ian M Berke, Lowella V Fortuno, Patrick D Skelton, and Ann Mae DiLeonardi

7. PERFORMING ORGANIZATION NAME(S) AND ADDRESS(ES)
DEVCOM Army Research Laboratory
ATTN: FCDD-RLA-HC
Aberdeen Proving Ground, MD 21005

8. PERFORMING ORGANIZATION REPORT NUMBER
ARL-TR-10024

9. SPONSORING/MONITORING AGENCY NAME(S) AND ADDRESS(ES)	10. SPONSOR/MONITOR'S ACRONYM(S)	11. SPONSOR/MONITOR'S REPORT NUMBER(S)

12. DISTRIBUTION/AVAILABILITY STATEMENT
DISTRIBUTION STATEMENT A. Approved for public release: distribution unlimited.

13. SUPPLEMENTARY NOTES
ORCID: Ian Berke, 0000-0002-6639-5506

14. ABSTRACT
Calcium imaging has become a popular approach for monitoring the activities of dynamic cellular networks. With recent imaging, molecular, and data processing advancements large calcium imaging datasets can now be analyzed with high throughput. Here, we implement our own approach using chemical and genetic calcium indicators paired with an open-source analysis package. These methods combine and extend previous algorithms for source-separation, calcium spike detection, and network synchronicity; and can be leveraged in a variety of experimental applications.

15. SUBJECT TERMS
Biological and Biotechnology Sciences, neuroscience, neural network, genetically encoded calcium indicator, machine learning

16. SECURITY CLASSIFICATION OF:			17. LIMITATION OF ABSTRACT	18. NUMBER OF PAGES
a. REPORT	b. ABSTRACT	C. THIS PAGE		
UNCLASSIFIED	UNCLASSIFIED	UNCLASSIFIED	UU	30

19a. NAME OF RESPONSIBLE PERSON	19b. PHONE NUMBER *(Include area code)*
Alexandra S Carrizales	(410) 306-0689

STANDARD FORM 298 (REV. 5/2020)
Prescribed by ANSI Std. Z39.18

Contents

List of Figures

1. Introduction

Calcium ions (Ca^{2+}) are ubiquitous second messengers that play a role in most cellular functions. In neurons, calcium flux is vital in the generation of action potentials (Brini et al. 2014). As such, these transients can serve as proxies for underlying electrical activity in neurons (Kim et al. 2014). There are two main classes of calcium indicators used to study calcium flux in neurons: 1) chemical and 2) genetically encoded indicators. While chemical indicators have a similar dynamic range to genetically encoded indicators, they are nonspecific and require repeated loading in chronic imaging experiments (Wu et al. 2019). Genetically encoded calcium indicators (GECIs) overcome these limitations by enabling cell-specific constitutive expression, which makes them favorable for long-term experimentation. The most widely used GECI, known as GCaMP, is composed of a green fluorescent protein (GFP) linked to calmodulin (CaM) and the M13 peptide from myosin light-chain kinase (Nakai et al. 2001). Upon calcium–calmodulin binding, GFP fluorescence increases. To deliver the GCaMP vector into target cells an Adeno Associated Virus (AAV) is leveraged. Cell type-specific expression is controlled both by viral serotype and upstream promoter. Currently the lab has many flavors of GCaMP, which can transduce neurons, astrocytes, or all cells.

While recent advancements in calcium indicators have improved our ability to monitor neural activity over extended time scales, quantifying these large datasets remains a challenge. Calcium imaging analysis can be broken down into five major steps: 1) image preprocessing, 2) motion correction, 3) cell and calcium signal extraction, 4) calcium event detection, and 5) network analysis. Historically, the gold standard approach to calcium imaging analysis has focused on manually identifying a subset of neurons from the population via user-defined traces and extracting the fluorescent signals of these few cells. Not only is this approach extremely tedious, but it can be biased as the activity patterns of a few cells might not be representative of the population. Additionally, this approach does not take full advantage of the spatiotemporal data structure. We take a holistic approach to calcium imaging analysis by simultaneously identifying neuron locations and demixing calcium signals of overlapping cells using a constrained non-negative matrix factorization (CNMF) framework. This enables efficient population activity tracking while minimizing computational times. Here, we present a comprehensive overview of calcium imaging and analysis methods that can be used to study the dynamic activities of neural ensembles.

2. Methods

2.1 Cell Culture

Isolated rat E18 hippocampi pairs were provided by TransnetYX Tissue. Isolated tissues were digested in 0.25% trypsin and DNase I diluted in Hank's Balanced Salt Solution and HEPES buffer solution. After incubating the tissues in the digestion solution at 37 °C for 20 min, the digestion solution was removed, and the tissues were washed three times with Neurobasal medium. Plating media (consisting of 2% B27, 2% fetal bovine serum, and 0.4-mM GlutaMAX) was then added to the tissues and the cells were dissociated by gently pipetting up and down with a P1000 micropipette. A cell strainer was used to filter the cell suspension prior to plating. Cells were plated on polyethyleneimine (PEI)-coated glass multielectrode arrays (gMEAs) at a density of 1.5×10^5 cells/cm^2. Cultures were maintained in the plating media and kept in the incubator at 37 °C and 5% CO_2. Half media (2% B27 and 0.4-mM GlutaMAX) exchanges were performed every 3–4 days.

2.2 Calcium Indicators

2.2.1 Chemical

Fluo-4 AM (ex./em. 488/540 nm; Invitrogen) was used as a chemical calcium indicator. This assay was prepared as prescribed in manufacturer documentation. Briefly, 100 µL of the cell medium was removed and replaced with 100 µL of Fluo-4 AM loading solution and incubated at room temperature for 20 min. Then, Fluo-4 AM loading solution was removed, and cultures were washed with the live cell imaging solution (LCIS; Invitrogen). Following washing, 100 µL of LCIS supplemented with 20-mM glucose was added to cells. The influence of probenecid (P; 1 mM) and Neuro-Background Suppressor (NBS; 1:10 dilution) were tested by incubating for 20 or 30 min prior to imaging. During each recording KCl (60-mM final concentration) was manually added at 30 s to test for a cellular response. Data was analyzed using ImageJ. Briefly, image stacks were corrected for photobleaching on an as-needed basis using the Bleach Correction plugin (Miura 2020). Next, a 2σ Gaussian kernel was applied in XYT and the first 100 stack images were used to calculate a mean baseline image (F_0), and $\Delta F/ F_0$ was calculated using standard image math for the entire field of view (Eq. 1).

$$\Delta F/F_0 = \frac{(F - F_0)}{F_0} \quad (1)$$

Where F represents raw fluorescence and F_0 represents baseline fluorescence.

2.2.2 Genetic

To transduce neuronal cultures, AAV (Addgene) was incubated with cells on day in vitro (DIV) 11. Then, 50% of culture medium was removed and cells were dosed with 1×10^{12} genome copies (GCs)/mL, which was determined following a preliminary dose response study (Fig. 1). During transduction, it is important not to disturb the growing neurons. We recommend dispensing the virus on one side of the culture vessel and gently rocking the plate back and forth to distribute the AAV. After the AAV was added, the cultures were placed in the 37 °C incubator for 1 h. Afterward, fresh feeding medium was added and the cultures were returned to the 37 °C incubator. Cultures were then supplemented with fresh feeding medium every 3–4 days via a 50% medium exchange. Prior to administering the AAV it is recommended to conduct a pilot study to determine the best titer for optimal transduction efficiency.

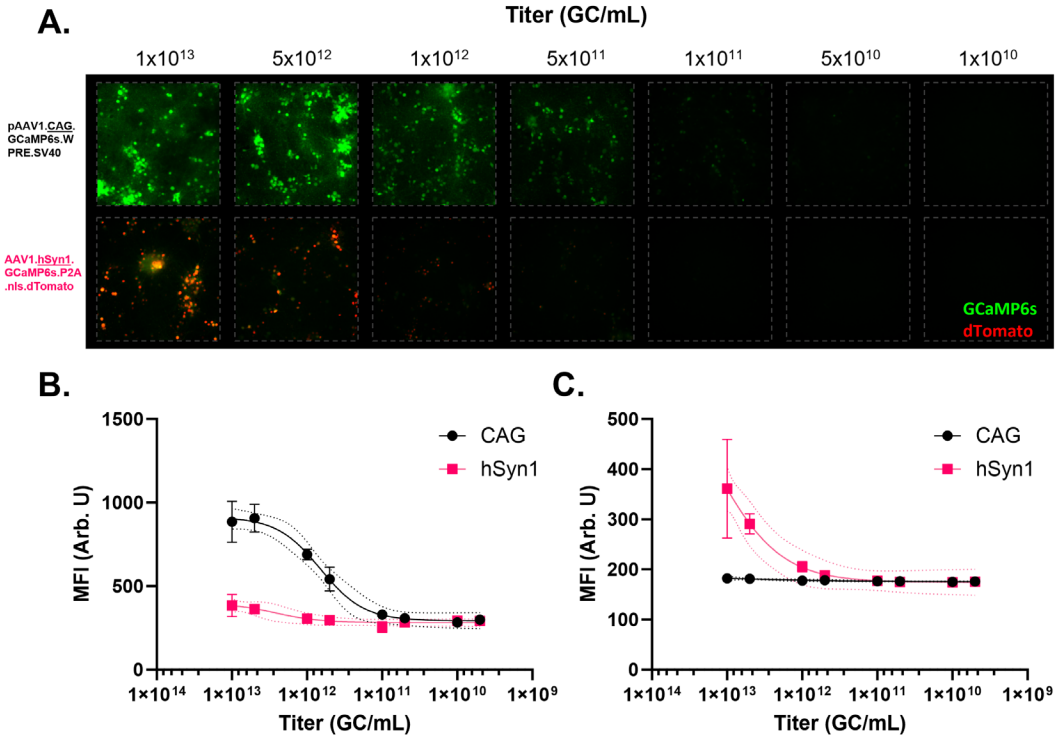

Fig. 1 An AAV dilution study was performed to determine appropriate viral concentrations for effective transduction prior to performing calcium imaging experiments. (A) Representative fluorescent images of transduced cultures on day in vitro (DIV) 15. Quantified mean fluorescent intensity (MFI) values are shown for (B) GCaMP6s and (C) dTomato channels. Sigmoidal fit ± 95% CI; n = 2/group mean ± SD.

We leveraged an AAV-hSyn1-GCaMP6s-P2A-nls-dTomato vector. The human synapsin 1 (hSyn1) gene promoter confers neuron-specific transgene expression, ensuring that only neurons in the culture will express the GCaMP construct. This version of GCaMP contains the GFP component, which has an excitation of

488 nm, as well as a separate dTomato (i.e., a red fluorescent protein with an excitation of 554 nm). By design, GCaMP expression of GFP is low in the neurons, making it difficult to gauge transduction efficiency without activating calcium flux. The addition of dTomato, provides easy detection on how efficiently the virus was transduced within the neural population because its intensity is independent of calcium concentration.

2.2.3 Calcium Imaging Data Acquisition

Wide-field calcium data was acquired via inverted epifluorescent Nikon Eclipse Ti equipped with a lumen core LED light source and Andor Zyla scMOS. A 470-nm laser was used for excitation with a 465–495 nm band pass excitation filter, a 505-nm high pass mirror, and a 515–555 nm emission filter. A stage-mounted temperature controller was used to maintain culture medium temperature at 37 °C during imaging. All calcium recordings were collected on DIV 19–21 and cultures were imaged for 5 min at 10 Hz. Data was saved in the native Nikon .nd2 format. To improve data quality, it is suggested that modern imaging systems that use multi-photon excitation or high-speed confocal acquisitions are leveraged if available (Berke et al. 2021).

2.2.4 Image Preprocessing

To preprocess the calcium recordings, the field of view (FOV) was down sampled from 2048 × 2048 pixels to 512 × 512 pixels using bicubic interpolation. While video dimension reduction is not a requirement for analysis, it can be used to reduce computation times. Down-sampled calcium recordings were saved as 16-bit BigTIFF stacks.

2.2.5 Motion Correction

Before extracting calcium signals from individual neurons, it is essential to ensure that each pixel corresponds to the same spatial location throughout acquired image stacks. To align video frames to a common template we implemented the nonrigid motion correction algorithm, NoRMCorre. This algorithm is designed to operate in either a rigid or piecewise-rigid manner depending on user specification. While rigid motion correction is usually sufficient for handling simple motion artifacts, the piecewise-rigid approach is recommended for correcting nonuniform motion artifacts, which are more prevalent in larger FOVs or within nonrigid tissues. Nonrigid motion artifacts are corrected by calculating motion vectors with subpixel resolution across overlapping patches within the video FOV (Pnevmatikakis and Giovannucci 2017). To initialize the algorithm, the user must specify a template image, which can either be a median image computed from the video or a structural

channel (e.g., TRITC). The algorithm splits the FOV into overlapping patches (of user-defined dimensions) and maps these patches to the template image.

In general, smaller patches are better at registering nonrigid transformations than larger patches, but it is important to consider features across the entire FOV before selecting a patch size. For example, if there are dark regions in the FOV (i.e., areas where there are not neurons), then a small patch may incorrectly estimate motion within that patch. For our analysis, we found a 128- × 128-pixel patch, with a 32-pixel overlap on both sides of adjacent patches effectively reduced motion artifacts (Fig. 2A). Other key parameters for the NoRMCorre algorithm are the maximum shift allowed for the entire FOV, and the maximum shift allowed for each patch in the X and Y directions. For the analysis presented here, the maximum FOV and patch shift were 10 and 5 pixels, respectively. Once motion correction was complete, data were saved to memory mapped files, which allows efficient data streaming. The memory mapping operation is a crucial step in analysis because it enables processing of large video files on a standard desktop.

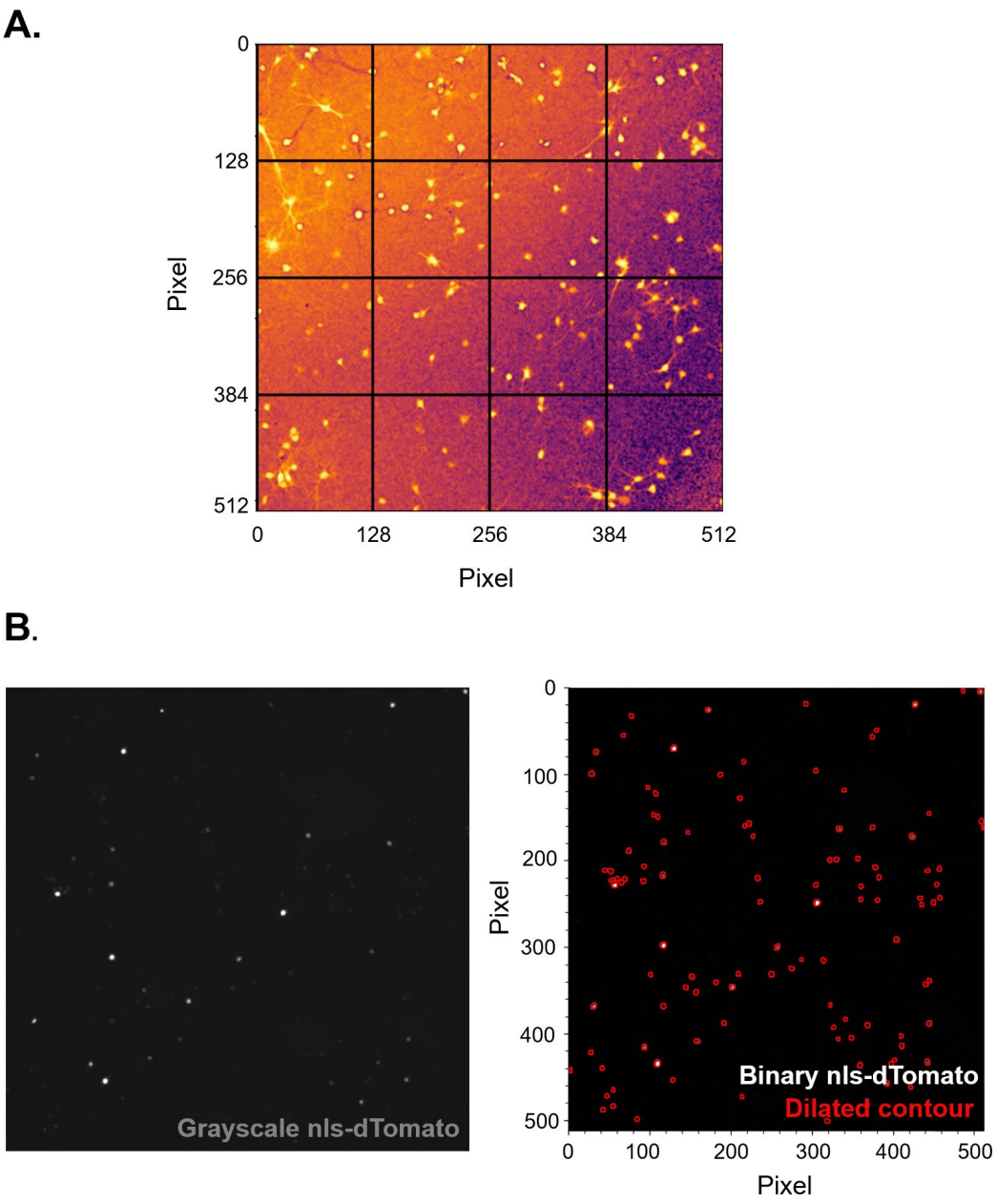

Fig. 2 Motion correction, parallelization, and segmentation approach. Patch size and example binary mask extraction for CNMF seeding. (A) Average image computed from calcium image stack with a FOV of 512 × 512 pixels partitioned into patches of size 128 × 128 pixels (shown in black). This patch size was utilized for both motion correction and parallel processing. (B) Grayscale nls-dTomato image (left) was thresholded using adaptive Gaussian thresholding and the nuclear regions of interest (ROIs) were dilated. Contours of the dilated ROIs are shown (right).

2.3 Neuron Detection and Calcium Signal Extraction

The spatiotemporal neuron data were extracted using CaImAn, a Python package for calcium imaging analysis (Giovannucci et al. 2019).

CNMF Framework

Neuron locations and calcium signals were extracted using a CNMF framework, which decomposes imaging data into the product of the spatial footprints of each neuron and their temporal components added to the product of the spatial and temporal components that correspond to the background. The CNMF framework is summarized by Eq. 2.

$$Y = AC + B + E \tag{2}$$

$Y \in \mathbb{R}^{d \times T}$ denotes the imaging data in matrix form, where d represents the total number of pixels in the FOV, and T is the number of frames in the imaging session. $A \in \mathbb{R}^{d \times N}$ denotes the spatial matrix, where N is the number of components, $A = [\mathbf{a}_1, \mathbf{a}_2, ..., \mathbf{a}_N]$, with $a_i \in \mathbb{R}^{T \times 1}$ corresponding to the spatial footprint of component i. $C \in \mathbb{R}^{N \times T}$ denotes the matrix of the temporal components, $C = [\mathbf{c}_1, \mathbf{c}_2, ..., \mathbf{c}_N]^{\mathrm{T}}$ with $c_i \in \mathbb{R}^{T \times 1}$ being the temporal trace for component i. The B term represents the background activity matrix. The background was modeled as a low rank matrix, $B = \mathbf{bf}$ where $\mathbf{b} \in \mathbb{R}^{d \times n_b}$ is the matrix of spatial background components, and $\mathbf{f} \in \mathbb{R}^{n_b \times T}$ is the matrix of temporal background components. Adjusting n_b allows the user to specify the number of global background components, which indicates the complexity of the background noise. For our analysis we set n_b equal to 3. Lastly, the E term represents the noise or residual error matrix, which captures the variability in the observed data that is not explained by the spatial footprints, temporal components, or background activity.

There are multiple strategies that can be used to initialize the CNMF framework. In the present study, we implement a seeded initialization approach, which enables input of a user-defined matrix of binary masks that outline cellular ROIs. Since our GCaMP6s construct included a dTomato tagged with a nuclear localization sequence, we utilized this channel to extract a binary mask for each neuron in the FOV. Adaptive Gaussian thresholding of this image with a specified kernel size (kernel size = 0.5*nuclear width) resulted in a binary image of segmented nuclei. Nuclear ROIs were then expanded to encompass the cytoplasm of each neuron using a morphological dilation with a 3- × 3-pixel structuring element. The resulting binary image was used to seed the CNMF framework (Fig. 2B). In some instances, background activity in calcium recordings can become too complex for the CNMF framework to handle. In these situations, the constrained non-negative

matrix factorization-endoscopic (CNMF-E) model can be used. While both methods have similar structures, CNMF-E estimates background activity as

$$B = W(Y - AC) \tag{3}$$

Here, W represents a weight matrix ($W \epsilon \mathbb{R}^{d \times d}$), where the (i, j) entry represents the influence of neuropil signal of pixel j on the neuropil signal of pixel i (Giovannucci et al. 2019). Essentially, the background at each pixel is represented as the weighted sum of the activity from a ring of pixels a certain distance from the reference pixel. The "ring_size_factor" parameter is used to specify the distance of the ring from the reference pixel. We found that a ring_size_factor of 1.5 was sufficient for our dataset. To initialize the CNMF-E framework the "GreedyCorr" method must be used. This initialization strategy uses correlation and the peak-to-noise ratio (PNR) to establish locations of candidate neurons. This approach first convolves the motion corrected calcium recording with a mean-centered Gaussian. The sigma of the Gaussian is specified by the "gSig" parameter (gSig = 0.5*neuron pixel diameter), and mean centering is done by setting the "center_psf" parameter to True. This operation creates a Gaussian with a positive peak in the middle and a width that is approximately half of the gSig parameter. The peak is surrounded by a negative trench with a ledge of zeros around the outer edges. The goal of this filtering approach is to reduce the influence of fluorescent changes occurring outside of the segmented soma ROI. Using the "correlation_pnr()" function, the mean-centered Gaussian is applied to each video frame, then correlation and PNR images are computed. The correlation image represents the correlation of each pixel with its neighbors, whereas the PNR ratio image is the ratio of the maximum magnitude at a pixel to the noise value at that pixel. The values in the correlation and PNR image are typically higher in pixels that contain neurons. Candidate neuronal pixels are seeded at the peaks in a product map created by setting a minimum peak threshold in the correlation image and the minimum PNR value in the PNR image (Giovannucci et al. 2019). Appropriate thresholds for correlation and PNR values must be determined by examining these computed images.

Compared to the seeded CNMF framework, the CNMF-E framework is much more computationally demanding. To help simplify the problem of neuron detection and calcium signal extraction, the FOV is split into overlapping patches of custom size that are processed in parallel. Processing in this manner reduces computational requirements and enables detection of neurons with smaller calcium transients without normalization (Giovannucci et al. 2019). Patches of 128 × 128 pixels worked well within our 512- × 512-pixel FOV. As with the motion correction operation, the density of the neural culture and the approximate sizes of the neurons are important considerations. Smaller patches provide higher spatial resolution, but

they can be more susceptible to noise; therefore, it is important to find balance between coverage and precision. Once all patches have been processed, they are embedded within the original FOV. Detected components that are spatially overlapping with highly correlated activity are merged. We found that a merge threshold of 0.85 worked well with our dataset.

3. Component Evaluation

Once candidate components have been detected and calcium signals have been extracted, it is important to filter the data to remove spurious components. There are three main criteria that can be used to evaluate candidate components:

1) Components are evaluated for their spatial footprint consistency. The spatial footprint consistency of a component is determined by correlating the footprint of the detected component with the average frame data during its active intervals. The calculated Pearson's correlation coefficient is then compared to the spatial threshold, and components that do not surpass this threshold are rejected from the dataset. We found that a spatial threshold of 0.8 was adequate for our dataset.

2) Components are evaluated for their peak signal-to-noise ratio (SNR). Here, we utilized the default SNR threshold of 2, which only accepts components that have a peak SNR across their temporal trace that is greater than 2.

3) Lastly, components are classified into neuron or non-neuron components using a pretrained four-layer convolutional neural network (CNN). This classifier assigns a value between 0 and 1 to each component depending on how well the component resembles a neuronal soma. Setting a minimum CNN threshold ensures the classifier only identifies a neuron if its associated probability meets or exceeds the threshold, increasing classification confidence and reducing false positives. We used a minimum threshold of 0.6 for our dataset. The CNN was trained on three manually annotated datasets collected from the hippocampus and cortex regions of the brain.[*]

3.1 Multisession Registration

Tracking the activity of neural populations across different imaging sessions is often an important aspect of calcium imaging experiments. To register neurons in the same FOV across different imaging sessions we implemented the Register

[*] http://neurofinder.codeneuro.org/

Multisession algorithm (available in CaImAn). This algorithm works by chronologically ordering imaging sessions and registering neurons identified in the first session to the neurons identified in the second session. The union of matched and unmatched components present in both sessions is kept and registered to the components present in the next imaging session. This process repeats until all imaging sessions have been registered. The FOV is aligned between imaging sessions and component registration between separate imaging sessions is conducted using an intersection over union metric to determine the distance between neighboring neurons. Cells that are above the specified maximum distance threshold are categorized as distinct. The default maximum distance threshold is 10 pixels; however, this scalar value can be adjusted to better suit the needs of the dataset. To ensure optimal matching between imaging sessions, the Hungarian algorithm was implemented to solve the linear assignment problem under the assumed distance function (Giovannucci et al. 2019).

3.2 Extraction of $\Delta F/F_0$

To obtain the normalized fluorescence trace corresponding to each neuron in GECI recordings the CaImAn function, "detrend_df_f()" was utilized. This function computes baseline fluorescence as a running percentile over a specified window. Here, we used the eighth quantile over a sliding window of 500 frames for the baseline calculation. The $\Delta F/F_0$ calculation is summarized in Eq. 1.

3.3 Calcium Event Detection

Although the CaImAn analysis package offers a deconvolution-based approach for detecting neuronal spike events, we found this strategy to be problematic when there is considerable background noise in the calcium recordings. For this reason, we relied on the SciPy package function "find_peaks()" to detect calcium spikes. This function identifies all local maxima in each calcium transient by comparing neighboring values across the signal. There are a variety of metrics that can be used to identify peaks within a signal, but we found the prominence and width parameters to be most effective. In the present study, prominence was set to 0.3 and the width was set to a range of 1–30 frames. These parameters may vary for different datasets; therefore, it is important to determine appropriate peak identification parameters experimentally. Identified peaks (spikes) were set to a value of one, while all nonpeak events were set to a value of zero resulting in a binary calcium spike matrix (of size neurons × frames) for our neural populations.

3.4 Calcium Spike Frequency

Individual neuron calcium spike frequency (Eq. 4) was computed by summing the total number of events detected for a given neuron and dividing by the movie duration in seconds.

$$\text{Spike Frequency} = \frac{spike\ count}{(recording\ duration)} \tag{4}$$

3.5 Network Synchronicity

Cultured neurons have been shown to exhibit synchronous activity patterns that cannot be captured via metrics such as spike frequency (Eisenman et al. 2015). To quantify this behavior, we implemented the phase synchronization approach described by Patel et al. (2015). Since this approach is based on instantaneous phase, we can strictly focus on the timing of calcium events independent of amplitude. Instantaneous phase was computed by "mapping" a full oscillatory cycle (phase angle from 0 to 2*pi) between consecutive spikes. This operation is summarized in Eq. 5.

$$\phi(t) = 2\pi * \frac{t - t^{(k)}}{t^{(k+1)} - t^{(k)}} + 2\pi k \tag{5}$$

Here, $t^{(k)}$ represents the spike time of the *kth* spike.

With the instantaneous phases, we then compute pairwise synchronization indices based on the circular variance of the pairwise instantaneous phase differences. The pairwise phase synchronization index calculation is summarized in Eq. 6.

$$\gamma_{i,j} = \sqrt{(\langle \cos(\phi_i(t) - \phi_j(t)) \rangle)^2 + (\langle \sin(\phi_i(t) - \phi_j(t)) \rangle)^2} \tag{6}$$

Here, brackets denote average over time.

Essentially, this calculation provides a measure of the variability in the distribution of the pairwise instantaneous phase differences when projected onto a unit circle. Pairwise phase synchronicity indices will take on a value between 0 and 1; where a synchronicity index of 0 indicates that the two signals are completely independent, and a synchronicity index of 1 indicates the two signals are perfectly synchronized. To compute a global synchronicity index representative of the entire population, we first perform eigen decomposition of the synchronization matrix to identify the number of unique activity patterns within the neural population. We then identify the largest eigenvalue, which is representative of the most dominant

synchronization pattern in the network. The global synchronicity index is then calculated by dividing the largest eigenvalue by the sum of all the eigenvalues.

3.6 Statistical Analysis

Statistical significance was calculated using Kruskal–Wallis nonparametric test with Dunn's posthoc test for pairwise comparisons between groups and adjusting for multiple comparisons using Bonferroni correction. An alpha value of 0.05 was considered statistically significant. Prior to the Kruskal–Wallis test, we checked the normality of the datasets using the Shapiro–Wilk test. Data were analyzed using Python 3.12.1 with the following packages: CaImAn 1.11.2, NumPy 1.26.3, pandas 2.1.4, SciPy 1.11.4, statsmodels 0.14.1, and Pingouin 0.5.4.

4. Results

4.1 Calcium Imaging

Various media additives were tested with Fluo-4 AM to determine their effects on calcium signal intensity and SNR. The addition of NBS was found to greatly improve the SNR (Fig. 3A) the addition of probenecid had a modest influence on Fluo-4 AM localization, which appeared to be more confined to cellular soma. Additionally, recovery toward the baseline was slowed (Fig. 3B), which can be seen as an increase in area under the curve (AUC). Incubation time did not overtly influence KCl-induced transients.

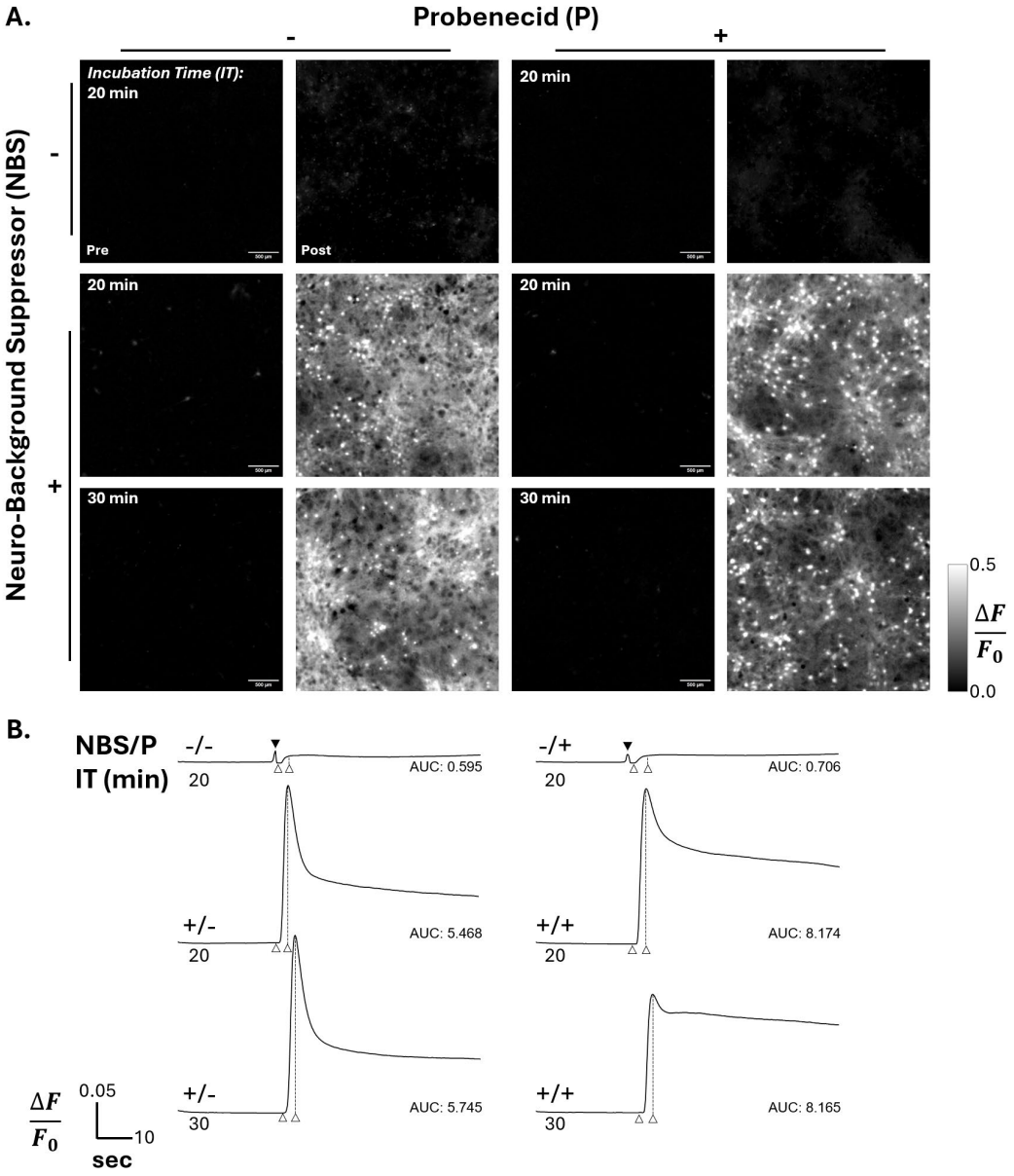

Fig. 3 Fluo-4 dye optimization experiments highlight the importance of media effects on calcium signal intensity. (A) Fluorescent images show the effect of Neuro-Background Suppressor (NBS) and Probenecid (P) with incubation times of 20 or 30 min, stills are shown pre- and post-addition of KCl. (B) Quantified $\Delta F/F_0$ traces show pre- and post-timepoints as indicated by open arrowpoints; closed arrowpoints highlight pipette-induced artifact in low signal-to-noise (SNR) recordings. Area under the curve (AUC) is shown for each trace.

4.2 Calcium Imaging Analysis

Using the NoRMCorre algorithm to correct for motion artifacts we implemented the piece-wise rigid approach. Although the rigid motion correction option is much faster, we chose to implement the piece-wise rigid method because it better detects nonuniform movements across the FOV. Additionally, the piece-wise rigid

approach splits the FOV across all axes and has been shown to outperform other nonrigid motion correction algorithms (e.g., Suit2p, SIMA, and Lucas–Kanade) that only split the FOV along a single axis (Pnevmatikakis and Giovannucci 2017).

Traditional approaches for identifying neuron locations have relied on the assumption that each pixel is assigned to a different neuron, which is often not the case. Networks of densely packed neurons can exhibit significant spatial overlap, and their calcium signals cannot be demixed using approaches like Independent Component Analysis (ICA), which rely on this linear assumption. Ignoring the spatial overlap would lead to significant "crosstalk" of signals, which could impact result interpretation (Pnevmatikakis et al. 2016). Therefore, we implemented a CNMF method, which is not limited to linear systems, to identify neuron spatial locations and extract calcium signals (Fig. 4A,B). Specifying prominence and width parameters for the find_peaks function, we were able to accurately detect calcium spikes (Fig 5A). Quantification of the calcium spike frequency revealed that each of our primary hippocampal networks had a median spike frequency ranging from 0.03 to 0.15 calcium spikes per second (Fig. 5B). This finding is consistent with prior studies that report similar spike frequencies (Boulware and Marchant 2008; Asthana et al. 2020; Voelker et al. 2021).

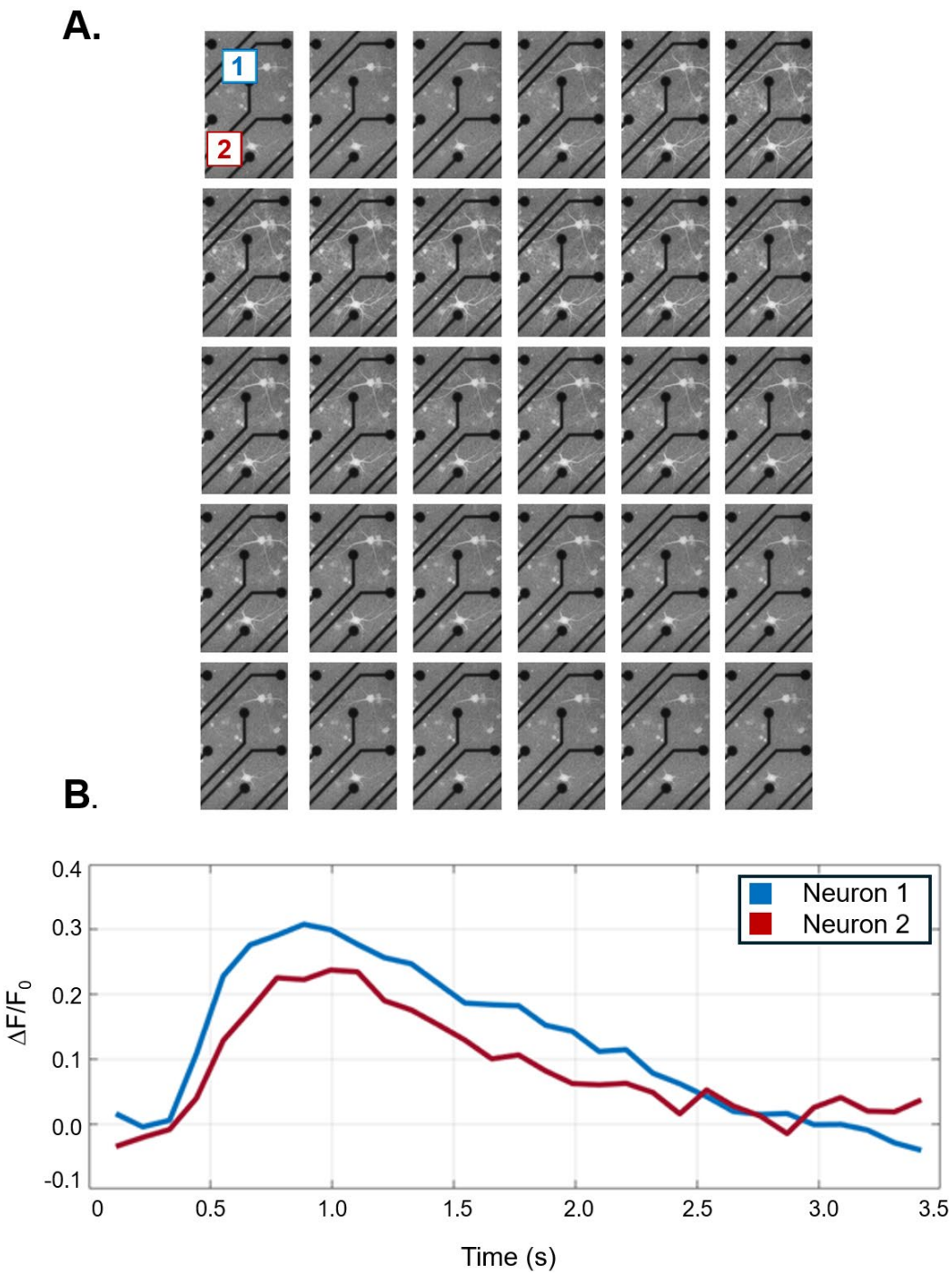

Fig. 4 Example GCaMP6s calcium spike. (A) Grayscale video frames showing change in GCaMP6s fluorescence during a single calcium spike for two example neurons labeled 1 and 2. Image frames are organized left to right and top to bottom. (B) Corresponding $\Delta F/F_0$ for neurons 1 and 2 are shown in the video frames.

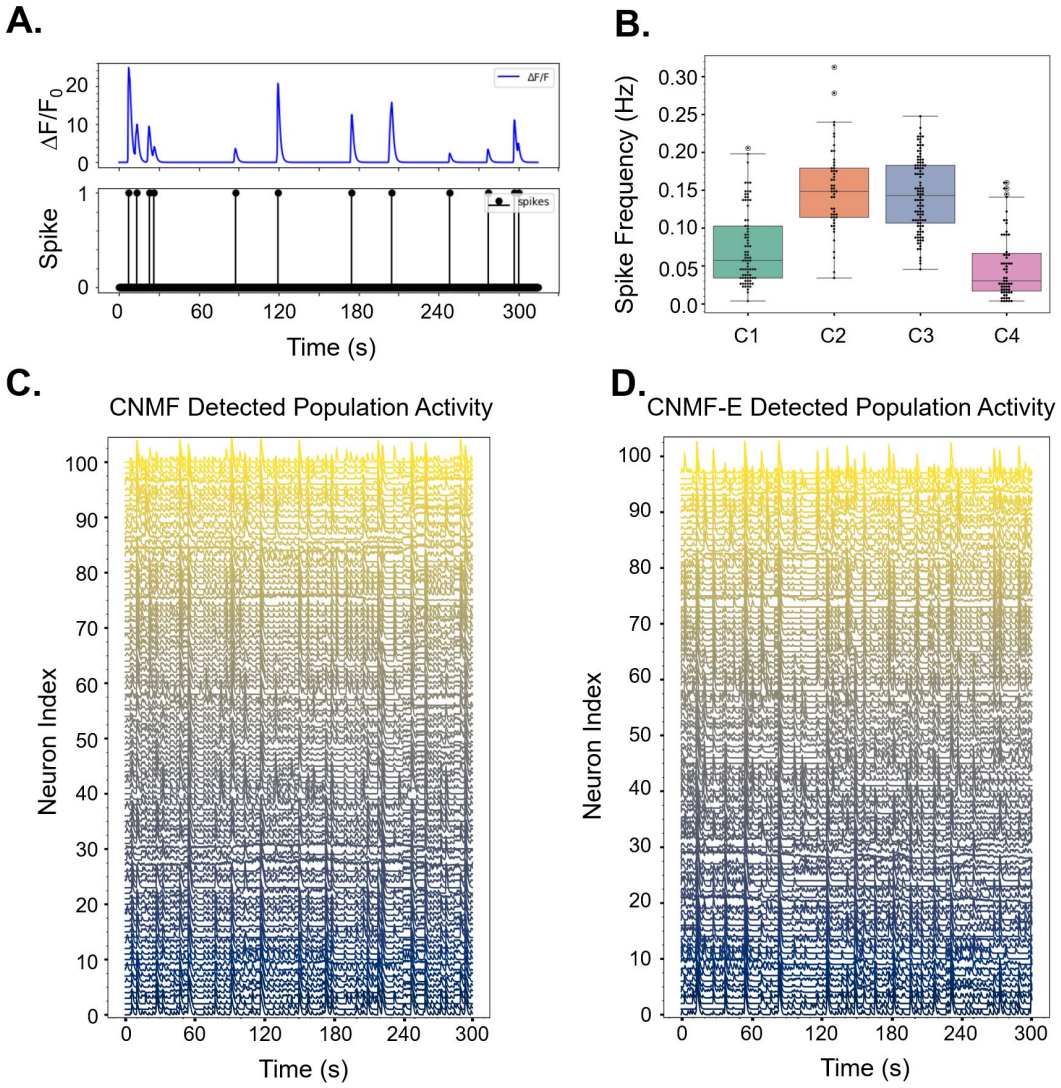

Fig. 5 Example calcium spike detection, population firing frequencies, and population activity. (A) Top: normalized calcium transient for a single neuron. Bottom: detected calcium peaks. (B) Box and whisker plot showing the distribution of calcium spike frequencies for four neural cultures (C1, C2, C3, C4). Black dots correspond to firing frequency of each neuron in the population. The open circles represent maximal or minimal outliers. Culture 1 vs. Culture 2 *, Culture 1 vs. Culture 3 ***, Culture 1 vs. Culture 4 **, Culture 2 vs. Culture 3 n.s., Culture 2 vs. Culture 4 ***, Culture 3 vs. Culture 4 ***. Statistical significance was determined via Kruskal–Wallis test with Dunn's posthoc test for pairwise comparisons between groups and adjusting for multiple comparisons using Bonferroni correction (*** $p < 0.001$, ** $p < 0.01$, * $p < 0.05$, n.s. = not significant). (C) Example population $\Delta F/F_0$ traces detected using CNMF or (D) CNMF-E frameworks.**

Although the CNMF framework was developed specifically for two-photon imaging, which typically has a higher SNR than one-photon wide field imaging (Denk and Svoboda 1997), we found that setting the number of background components (n_b) to three was sufficient for most of our calcium recordings (Fig. 5C). In some instances, the background activity was too complex to be

modeled by the CNMF framework; for these cases we employed the CNMF-E framework (Fig. 5D). While the CNMF-E framework is better suited for handling complex background activity, it is important to note that both the CNMF and CNMF-E frameworks can struggle when calcium activity is sparse, such as following injury. In these instances, the CNMF or CNMF-E frameworks can still be used to identify neural spatial footprints from a calcium recording collected prior to the injury. However, we recommend aligning these spatial footprints to the FOV of the image stacks and then extracting the average pixel intensities for these regions across time using a custom Python script.

Using the register multisession algorithm, we were able to accurately track neural activity imaged at two different time points (Fig. 6). Although our study did not involve activity tracking before and after treatment administration, this algorithm can be particularly useful in such cases.

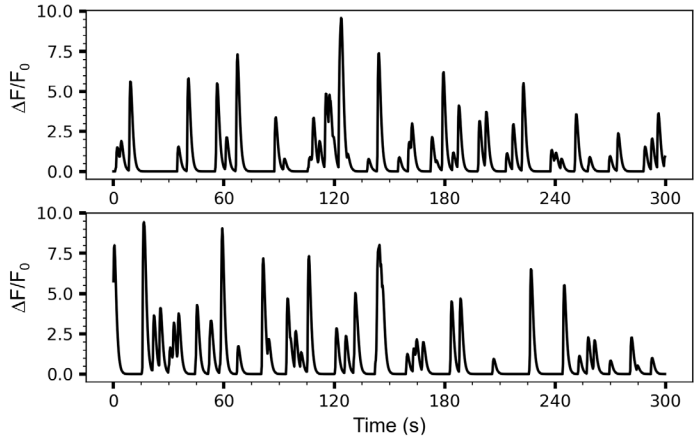

Fig. 6 Example tracking of neuron activity across two imaging sessions. $\Delta F/F_0$ for a neuron detected during the initial imaging session (top) and during a subsequent imaging session (bottom). Neuron activity tracking across the two imaging sessions was achieved using the Register Multisession algorithm.

4.3 Network Synchronicity

Activity synchronization is a key feature of living neural networks that has been shown to play a role in efficient information transfer and in some cases pathophysiological conditions (Uhlhaas and Singer 2006). Using the instantaneous phase-based approach to compute network synchronicity (Fig. 7A), we observed a variety of synchronization patterns (Fig. 7B) across our cultures with global synchronicity ranging from 0.15 to 0.35 (Fig. 7C). Importantly, using a single metric (global synchronicity index) to represent a population's synchrony may ignore other more complex attributes of the network (i.e., sub-ensembles/networks), which may be apparent in a pairwise phase synchronization matrix.

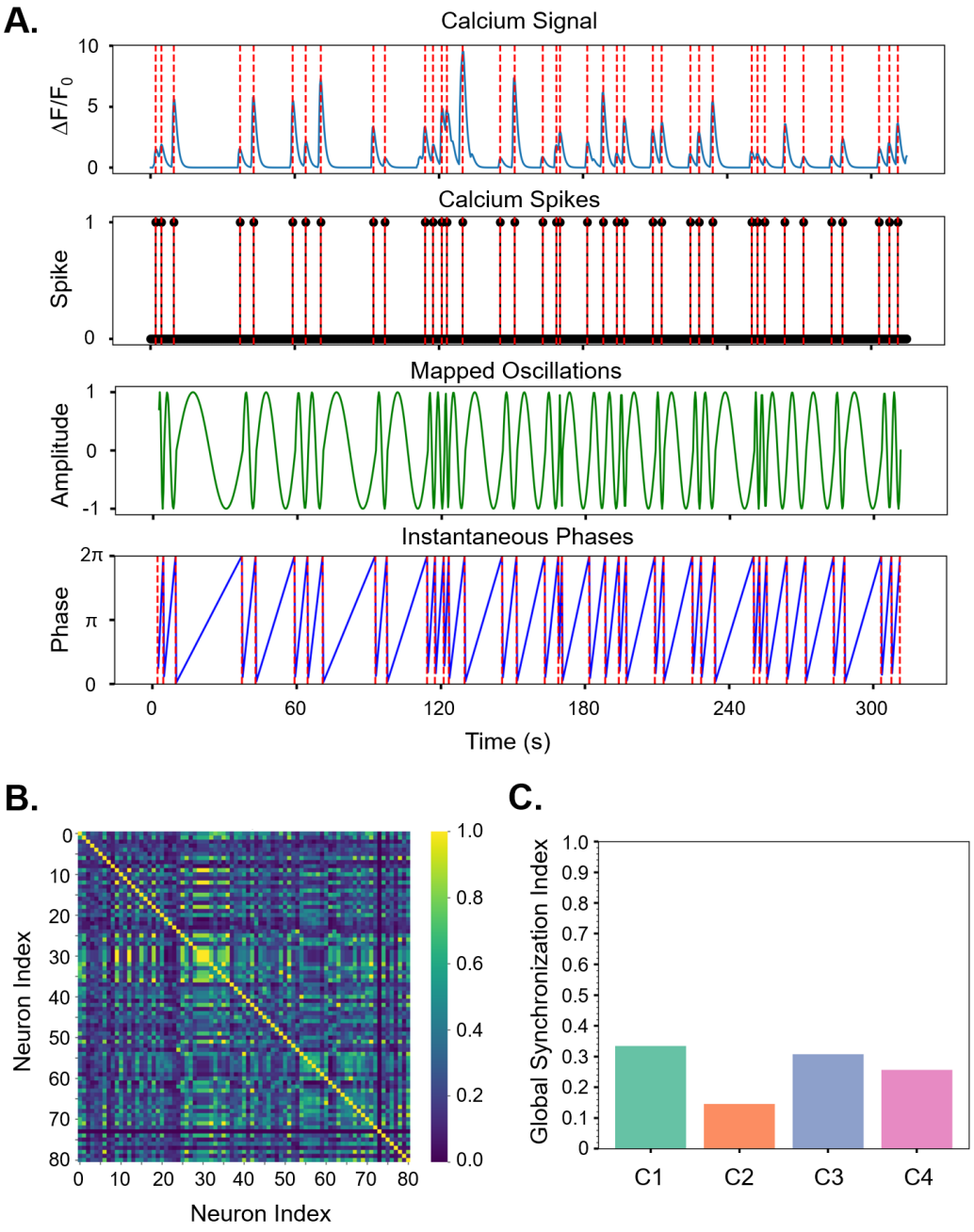

Fig. 7 Example network phase synchronization. (A) Mapping of full oscillations between consecutive spikes used to obtain the instantaneous phases of the signal. (B) Example pairwise phase synchronization matrix for neural culture 1 (C1). (C) Computed global synchronicity indices for four example neural cultures (C1, C2, C3, C4).

5. Conclusion

Calcium imaging and analysis are crucial experimental methods in understanding neural dynamics. In the present study we provide an overview of calcium imaging and analysis methods using Fluo-4 AM and GCaMP6s, and an open-source calcium imaging analysis package, CaImAn. While we demonstrate the use of these methods in control populations, they can easily be adapted to a variety of experimental applications. These methods provide a robust framework for understanding neuronal activity, offering valuable insight for basic neuroscience research and clinical applications. Future work will aim to expand on these methods to better understand the complex behaviors of neural networks. This includes adding capabilities for computing neuron correlations, calculating the area under each calcium peak, and identifying neurons that participate in synchronous clusters.

6. References

Asthana A, Ndyabawe K, Mendez D, Douglass M, Haidekker MA, Kisaalita WS. Calcium oscillation frequency is a potential functional complex physiological relevance indicator for a neuroblastoma-based 3D culture model. ACS Biomaterials Science & Engineering. 2020;6(7):4314–4323. https://doi.org/10.1021/acsbiomaterials.9b01988

Berke IM, McGrath TM, Stivers JJ, Gui C, Barcellona MN, Gayoso MG, Tang SY, Cao YQ, Gupta MC, Setton LA. Electric field stimulation for the functional assessment of isolated dorsal root ganglion neuron excitability. Ann Biomed Eng. 2021;49:1110–1118. https://doi.org/10.1007/s10439-021-02725-y

Boulware MJ, Marchant JS. Timing in cellular Ca^{2+} signaling. Current biology: CB. 2008;18(17):R769–R776. https://doi.org/10.1016/j.cub.2008.07.018

Brini M, Calì T, Ottolini D, Carafoli E. Neuronal calcium signaling: function and dysfunction. Cellular and Molecular Life Sciences: CMLS. 2014;71(15):2787–2814. https://doi.org/10.1007/s00018-013-1550-7

Denk W, Svoboda K. Photon upmanship: why multiphoton imaging is more than a gimmick. Neuron. 1997;18(3):351–357. doi:10.1016/s0896-6273(00)81237-4

Eisenman LN, Emnett CM, Mohan J, Zorumski CF, Mennerick S. Quantification of bursting and synchrony in cultured hippocampal neurons. J Neurophysiol. 2015;114(2):1059–1071. https://doi.org/10.1152/jn.00079.2015

Giovannucci A, Friedrich J, Gunn P, Kalfon J, Brown BL, Koay SA, Taxidis J, Najafi F, Gauthier JL, Zhou P, et al. CaImAn - an open source tool for scalable calcium imaging data analysis. Elife. 2019;8:e38173. https://doi.org/10.7554/eLife.38173

Kim DS, Jayaraman V, Looger LL, Svoboda K. Engineering fluorescent calcium sensor proteins for imaging neural activity. Society for Neuroscience. 2014. http://www.sfn.org/~/media/SfN/Documents/Short%20Courses/2014%20SC%201/SC%201%20Chapters/Douglas%20Kim.ashx

Miura K. Bleach correction ImageJ plugin for compensating the photobleaching of time-lapse sequences. F1000Res. 2020 Dec 21;9:1494. doi: 10.12688/f1000research.27171.1. PMID: 33633845; PMCID: PMC7871415

Nakai J, Ohkura M, Imoto K. A high signal-to-noise Ca^{2+} probe composed of a single green fluorescent protein. Nat Biotechnol. 2001;19:137–141. https://doi.org/10.1038/84397

Patel TP, Man K, Firestein BL, Meaney DF. Automated quantification of neuronal networks and single-cell calcium dynamics using calcium imaging. J Neurosci Methods. 2015;243:26–38. https://doi.org/10.1016/j.jneumeth.2015.01.020

Pnevmatikakis EA, Soudry D, Gao Y, Machado TA, Merel J, Pfau D, Reardon T, Mu Y, Lacefield C, Yang W, et al. Simultaneous denoising, deconvolution, and demixing of calcium imaging data. Neuron. 2016;89(2):285–299. https://doi.org/10.1016/j.neuron.2015.11.037

Pnevmatikakis EA, Giovannucci A. NoRMCorre: an online algorithm for piecewise rigid motion correction of calcium imaging data. J Neurosci Methods. 2017;291:83–94. https://doi.org/10.1016/j.jneumeth.2017.07.031

Uhlhaas PJ, Singer W. Neural synchrony in brain disorders: relevance for cognitive dysfunctions and pathophysiology. Neuron. 2006;52(1):155–168. https://doi.org/10.1016/j.neuron.2006.09.020

Voelker J, Voelker C, Engert J, Goemann N, Hagen R, Rak K. Spontaneous calcium oscillations through differentiation: a calcium imaging analysis of rat cochlear nucleus neural stem cells. Cells. 2021;10(10):2802. https://doi.org/10.3390/cells10102802

Wu N, Nishioka WK, Derecki NC, Maher MP. High-throughput-compatible assays using a genetically-encoded calcium indicator. Sci Rep. 2019;9:12692. https://doi.org/10.1038/s41598-019-49070-8

List of Symbols, Abbreviations, and Acronyms

AAV	Adeno Associated Virus
AUC	area under the curve
Ca^{2+}	calcium ions
CaM	calmodulin
CNMF	constrained non-negative matrix factorization
CNMF-E	constrained non-negative matrix factorization-endoscopic
CNN	convolutional neural network
DIV	day in vitro
FOV	field of view
GC	genome copy
GECI	genetically encoded calcium indicator
GFP	green fluorescent protein
hSyn1	human synapsin 1 (gene promoter)
gMEA	glass multielectrode array
ICA	Independent Component Analysis
LCIS	live cell imaging solution
LED	light-emitting diode
NBS	Neuro-Background Suppressor
n.s.	not significant
P	Probenecid
PEI	polyethyleneimine
PNR	peak-to-noise ratio
ROI	region of interest
SNR	signal-to-noise ratio

1 (PDF)	DEFENSE TECHNICAL INFORMATION CTR DTIC OCA
1 (PDF)	DEVCOM ARL FCDD RLB CI TECH LIB